https://doi.org/10.20965/jdr.2018.p0472

Paper:

Onboard Realtime Processing of GPS-Acoustic Data for Moored Buoy-Based Observation

Motoyuki Kido[*1,†], **Misae Imano**[*2], **Yusaku Ohta**[*2], **Tatsuya Fukuda**[*3], **Narumi Takahashi**[*4], **Satoshi Tsubone**[*5,3], **Yasuhisa Ishihara**[*3], **Hiroshi Ochi**[*3], **Kentaro Imai**[*6], **Chie Honsho**[*2], **and Ryota Hino**[*2]

[*1]International Research Institute of Disaster Science, Tohoku University
468-1 Aza-aoba, Aramaki, Aoba-ku, Sendai 980-8572, Japan
[†]Corresponding author, E-mail: kido@irides.tohoku.ac.jp
[*2]Graduate School of Science, Tohoku University, Sendai, Japan
[*3]Marine Technology and Engineering Center, Japan Agency for Marine-Earth Science and Technology, Yokosuka, Japan
[*4]Earthquake and Tsunami Research Division, National Research Institute for Earth Science and Disaster Resilience, Tsukuba, Japan
[*5]Interlink Inc., Nagoya, Japan
[*6]Research and Development Center for Earthquake and Tsunami, Japan Agency for Marine-Earth Science and Technology, Yokohama, Japan

[Received December 26, 2017; accepted March 27, 2018]

Realtime observations of vertical/horizontal seafloor movements and sea surface height associated with a huge earthquake are crucial for immediate recognition of its causal fault rupture, so that tsunami early warning can be issued and also the risk of subsequent ruptures can be evaluated. For this purpose, we developed an offshore monitoring system using a moored buoy platform to measure, in realtime, the three observables mentioned above and operated it on a trial basis for a year. While operating the system, GPS-acoustic observation of horizontal movement on the buoy was especially a new challenge. To achieve realtime GPS-acoustic observation under conditions of the limited power supply and narrow bandwidth in satellite communication, we developed special hardware suitable for use on a buoy and software to minimize onboard computational procedures and data transmission. The system functioned properly through the year; 53 regular weekly measurements and 55 on-demand measurements at arbitrary timings. Each measurement consisted of 11 successive acoustic rangings. The buoy tended to drift far from the preferred position for GPS-acoustic measurement, i.e., the center of the seafloor transponder array, due to strong current. The accuracy of the GPS-acoustic positioning achieved ∼46 cm (2σ) even only with "a single ranging" when the buoy was inside the array, while it degraded to ∼1.0 m when the buoy was outside the array. Although the 1.0 m accuracy is a detectable level of possible displacement due to a M8-class earthquake in the source region, further improvement to keep the drifting range smaller despite the current will enhance the utilization of the system.

Keywords: realtime monitoring, buoy, GPS-acoustic, tsunami, Nankai Trough

1. Introduction

Huge earthquakes and accompanying tsunamis are devastating disasters which mostly occur along subduction zones beneath the ocean. To devise effective safety measures, it is important to assess seismic risk based on geophysical observations and numerical simulations (e.g., [1, 2]). However, immediate detection of disaster is also crucial to mitigate consequent damages, particularly to human lives [3]. Therefore, many efforts have been made, in recent years, to construct offshore monitoring systems, especially using geodetic techniques. In this section, we first introduce currently-available offshore geodetic monitoring systems and then explain the development history of the GPS-acoustic technique, which is the main component of a new system that we propose.

1.1. Ongoing Offshore Geodetic Monitoring

Realtime monitoring of a rapid change of offshore sea surface height provides the most direct information on tsunami generation preceding its arrival to the coast. Kato et al. [4] have developed a GPS-buoy that allows for precise measurement of its ellipsoidal height using "Real-Time Kinematic" (RTK) analysis of GPS data. After removal of fluctuation of the height due to surface wave by taking its temporal average, net sea surface height can be monitored. Up to 18 GPS-buoys are currently in operation, surrounding the Japanese islands as a part of the "Nationwide Ocean Wave information network for Ports and HArbourS" (NOWPHAS) system [5] for wave and tsunami monitoring. Onboard RTK analysis requires onshore fiducial GPS data for differentiation, the data rate of which is too large to transmit using satellite communication. Therefore, the GPS-buoy employs UHF terrestrial communication, which limits the distance to which the buoy can be stationed from the coast to <20 km. Recently, Terada et al. [6] overcame this limit by employing the "Precise Point Positioning with Ambiguity Resolution" (PPP-AR) technique [7], which needs only correction information via satellite.

Static pressure on the ocean bottom is, basically, the weight of a water column of a unit cross-section and reflects changes in sea surface height and/or vertical movements of the seafloor. Offline "Ocean Bottom Pressure" (OBP) gauges are popular for scientific purposes (e.g., [8]); however, realtime data transmission is required for disaster mitigation. The most straightforward way to enable this is to connect OBP gauges to a seafloor cable that connects them to an onshore station. Large-scale examples are the "Dense Oceanfloor Network system for Earthquakes and Tsunamis" (DONET1/DONET2) installed off the Kii-peninsula along the Nankai Trough [9–11], and the "Seafloor observation Network for Earthquakes and Tsunamis along the Japan Trench" (S-net) [12]. Seafloor cables contain optical networks with adequate bandwidth for data transmission and can supply electric power to instruments to enable semi-permanent operation. A more cost-effective and freely installed system is "Deep-ocean Assessment and Reporting of Tsunamis" (DART), in which OBP data are relayed via acoustic modem to a surface buoy, which is tautly moored near the OBP, and are then forwarded via satellite communication to an onshore station [13]. DART buoys are globally operated, mainly along the circum-Pacific subduction zones and partially in the Indian and Atlantic Oceans.

These densely distributed realtime OBP data enable us to recognize a tsunami source at an early stage of tsunami generation. Tsushima et al. [14] proposed "tsunami Forecasting based on Inversion for initial sea-Surface Height" (tFISH), which inverts time-series of OBP data into initial sea surface heights as a tsunami source, and then forwardly computes tsunami waveform at any time stage. Further improvement of tFISH is in progress, through the incorporation of onshore GPS-based fault modeling ("Real-time Automatic detection method for Permanent Displacement" (RAPiD) [15]) as an initial source [16].

All the monitoring systems addressed above are based on offshore OBP or sea surface height data [17]. No horizontal seafloor movement is incorporated at present because this data can only be measured by the GPS-acoustic (GPS-A) technique, which usually employs campaign-style surveys; moreover, obtained data must be analyzed through post-processing. Although vertical crustal movement efficiently contributes to generating tsunamis, horizontal movement is usually much larger than vertical one because of the smaller dip angles of the plate interfaces. Thus, horizontal movement observed by GPS-A measurements potentially plays an important role in constructing a fault slip model.

1.2. Introduction of GPS-A Technique

GPS-A technique, pioneered by the Scripps Institution of Oceanography in the USA [18], measures the position of seafloor benchmarks by combining kinematic GPS analysis of a sea surface platform and acoustic ranging to the seafloor benchmarks using round trip traveltimes of active sonar. Following the first practical scientific result at the Juan de Fuca plate [19], the technique was imported and further developed by Japanese research groups and has been applied to measuring the secular and coseismic displacements along subduction zones surrounding the Japanese islands. For example, 20–30 cm of coseismic displacement associated with the 2004 Off the Kii Peninsula earthquake was independently observed [20, 21]. The sequence of secular, coseismic, and postseismic seafloor deformations were first observed for the 2005 Off-Miyagi Prefecture earthquake [22–25].

One of the most prominent contributions that highlights the advantage of GPS-A is detection of the coseismic displacement of the 2011 Tohoku earthquake immediately above its source region [26, 27]. This led the Japanese government to deploy extensively geodetic networks of GPS-A on the seafloor, especially in shallower dip areas, as well as to construct the S-net described above. The newly installed GPS-A network along the Japan Trench revealed the distribution of postseismic movement following the Tohoku earthquake, mostly due to postseismic slips and viscoelastic responses [28–30]. Along the Nankai Trough, a GPS-A network was also extended toward the trench side, which contributed to elucidating the distribution of coupling conditions of the plate interface [31–33].

However, traditional GPS-A surveys have the following restrictions that conflict with realtime monitoring: campaign-style surveys can be conducted only when visiting with a research vessel, nearly 24 hours of data stacking is required to reduce the effect of unwanted error sources, and also controlled ship track or point-keeping is required during a survey. Kido et al. [34] introduced a self-powered Autonomous Surface Vehicle (ASV) and a moored buoy as surface platforms for continuous GPS-A surveys, but these were still in the trial phase and lasted only for a couple of days at the time of their study. Recently, Chadwell [35] employed a wave-powered surface vehicle (Wave Glider) and succeeded in conducting repeated campaign surveys in the Cascadia subduction zone. However, a Wave Glider can stay on a controlled track or a fixed point only in regions with weak sea current. In the region of the western intensification of boundary currents, such as the Kuroshio or Kuroshio Extension, it is difficult to always stay at the site under control. A slackly moored buoy is a practical solution in such a situation. In this case, it is getting important to carefully evaluate the accuracy of GPS-A positioning only with "a single ranging" from "an arbitrary position" within the drifting range of the buoy. In the past three years, we have developed such a buoy and performed sea trials under the Strategic Innovation Promotion Project (SIP), to provide on-demand monitoring of tsunami and vertical/horizontal crustal movements immediately after a possible M8-class earthquake.

In this paper, we focus on realtime GPS-A measurement among the entire buoy system, especially in techni-

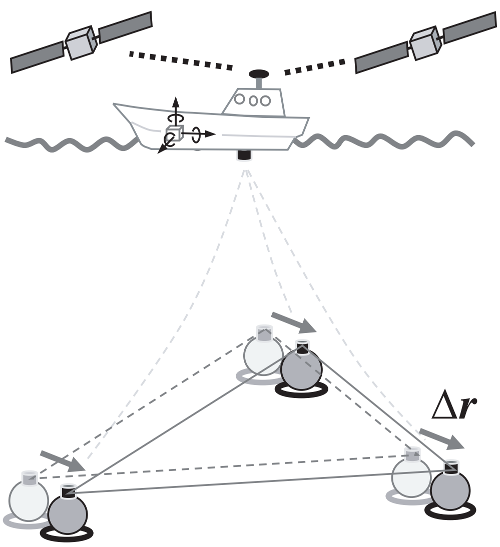

Fig. 1. A typical GPS-acoustic point survey scheme. Three or more seafloor precision transponders (PXPs) form an array. Simultaneous ranging to all the PXPs determines horizontal array position and averaged sound speed variation. The position and attitude of a surface platform are monitored using kinematic GPS and a gyroscope.

Table 1. Comparison of moving and point surveys with various aspects.

Survey style	Moving survey (3–6 PXPs)	Point survey (3–4 PXPs)	Point survey (6 PXPs)
Surface platform	Ship, ASV	Ship, ASV, Wave Glider, Buoy	
Measured target	Horizontal, Vertical, Array shape	Horizontal	Horizontal, Vertical*1
Realtime capability (Min. time)	× (several hours)	○ (1 min)	○ (1 min)
Accuracy (2σ, 1 min, inside array)	N/A	∼46 cm*2	∼46 cm*2
Accuracy (2σ, 1 min, outside array)	N/A	Inf.	∼100 cm*2
Accuracy (2σ, 12hours, optimum position/track)	∼5 cm	∼5 cm	∼5 cm

*1 Only when survey position remains inside optimum location range.
*2 Discussed in Section 4.3.

cal aspects. We first propose a method of analysis suitable for a single ranging from an arbitrary position. Then, the design of hardware and software of the GPS-A system on the buoy is introduced. Finally, positioning accuracy is discussed, using observed data from a yearlong mooring operation.

2. GPS-Acoustic Measurement

2.1. Principle of GPS-A Measurement

As the GPS-A measurement is a combination of kinematic GPS analysis of a surface platform and underwater acoustic ranging to seafloor precision transponders (PXPs), positioning accuracy relies upon how accurately determining the sound speed in seawater. In general, sound speed structure in ocean can be well approximated using a time-dependent laterally stratified model. At least three PXPs as a set are required which usually form a regular polygon called an "array," as shown in **Fig. 1**, the dimension of which is roughly equal to depth of the site. Assuming the geometry of the array remains rigid through campaigns, one can solve the horizontal position of the array and average sound speed through the water column as a function of time or each ranging epoch [18].

Two survey styles are widely employed. One is the "moving survey" (e.g., [22]), in which a surface platform repeatedly moves over the array, gathering acoustic paths with various azimuths and nadir angles as many as possible. With this approach, vertical crustal motion and change in array geometry (initial uncertainty or internal seafloor deformation within the array), if any, can be also solved at least in principle, in addition to horizontal array position and sound speed variation. The other style is "point survey" (e.g., [18]), in which a surface platform is kept staying just above the center of the array. The point survey only measures relative inter-campaign movement of horizontal array position and cannot distinguish vertical movement from sound speed variation. However, the point survey method can intrinsically determine the horizontal position of the array only using a single ranging, which is an indispensable characteristic for realtime monitoring. Therefore, we employed the point survey method in our research for realtime monitoring and describe the principle in detail in the next section. The features of moving and point surveys are summarized in **Table 1**.

2.2. Point Survey

Spiess [18] demonstrated that temporal variation in sound speed does not affect horizontal array positioning as long as sound speed structure is stratified and point survey is made exactly at the center of the array. However, vertical movement and change in sound speed cannot be distinguished because of their fully equivalent effect on traveltimes. Kido et al. [36] introduced a scalar quantity to represent sound speed variation: "vertically normalized traveltime residual" or "Nadir Total Delay" (NTD), which can extend the flexibility of the measurement, allowing the survey position to deviate from the array center. The tolerable range of deviation depends on the accuracy of the initial determination of the array geometry. Furthermore, even if the survey position significantly deviates from the center, apparent inter-campaign relative motion is not affected as long as it keeps the same position throughout the campaigns. This is because the deviation always produces the same error, which will cancel itself out after differentiation.

Although the point survey can solve array position using a single ranging, a typical campaign survey with a research vessel usually takes a temporal average of the solutions for nearly 24 hours to remove unwanted errors, such as uncertainty in GPS analysis, attitude of the ves-

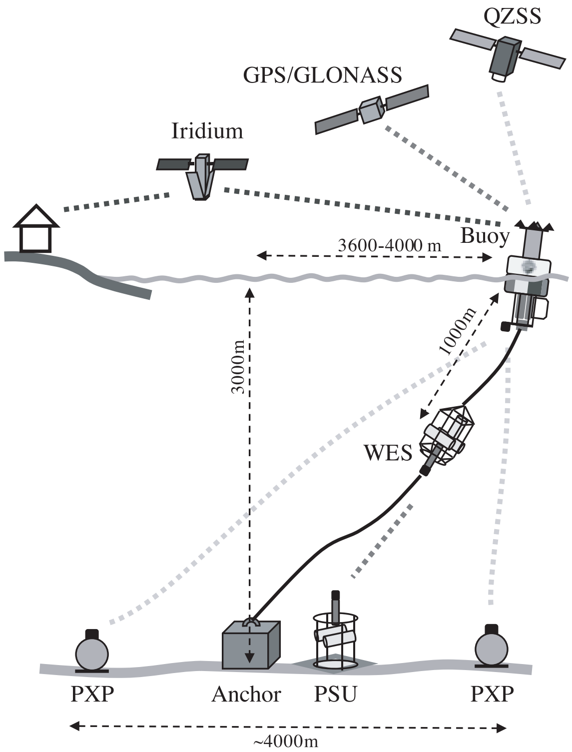

Fig. 2. A schematic illustration of the moored buoy system (not to scale). The buoy receives GNSS signals from GPS/GLONASS and QZSS satellites. Data transmission to an onshore station is conducted by Iridium satellite communication. Pressure data are observed by a Pressure Sensor Unit (PSU) at the bottom and relayed to the Wire End Station (WES) using an acoustic double pulse, then transferred to the buoy in parallel through an inductive modem and wired serial communication. A total of six PXPs were installed on the seafloor for GPS-acoustic measurement.

sel, traveltime detection, and horizontal sound speed variation. Among the above, horizontal sound speed variation is the most significant. If typical timescale of this variation is much shorter than the duration time of a campaign survey, its effect will be efficiently reduced. Gravitational internal wave, which is often excited by the interaction of tidal flow with seafloor topographic bump, generates oscillation of stratified layers in time and space. The oscillation period is limited by Väisälä frequency depend on density gradient in a water column, which is typically shorter than one hour. On the contrary, persisting horizontal variation occasionally came across at the edge of an eddy or strong current, which behaves a long-lasting bias and cannot be reduced by temporal average. This kind of persisting horizontal variation in sound speed structure can be evaluated and removed by moving survey. However, it falls into apparent array movement in the point survey or realtime monitoring. Kido [37] deduced that horizontal gradient can be removed even by point survey using five or more PXPs, which has not achieved an effect yet in real observed data. Thus, the realtime monitoring using a moored buoy intrinsically contains these errors.

3. System

3.1. Hardware

3.1.1. Moored Buoy

Since our moored buoy system has already been introduced in its prototype [38, 39] and most recent version [40], we briefly describe here the essential functions of the system in **Fig. 2**. The main body is 5 m in height. At the top, an Iridium communication antenna, meteorological sensor, and totally five GNSS antennas respectively compliant with GPS, GLONASS, and QZSS are installed. Electric power is supplied by solar panels surrounding the main electronics box. Below the draft, an Acoustic Doppler Current Meter (ADCM), acoustic transducer for GPS-A, and pressure tight cases containing electronics and batteries are equipped. The main body is connected to a Wire End Station (WES) below 1000 m, which receives pressure data from the seafloor Pressure Sensor Unit (PSU) close to the anchor with a small acoustic signal in the nearly noiseless environment. The buoy is slackly moored with a cable via a slip ring that allows free rotation even containing signal and power lines inside. The slack ratio (total cable length over depth) is $4700\ \mathrm{m}/3000\ \mathrm{m} = 1.57$, which is a lower limit for our present buoy given a current over 5.5 knots. Six PXPs for GPS-A are on the seafloor arranged in a triangle, the dimension of which is nearly the same as its depth ($\sim$3000 m). The electronics inside the buoy relevant to GPS-A are briefly illustrated in **Fig. 3** and are described in the following subsections.

3.1.2. GNSS and Gyro

The buoy is equipped with three GNSS receivers: Trimble MB-One, JAVAD Delta-3, and JAVAD SigmaQ, as fallback systems to each other. MB-One provides precise positioning data at 10 Hz through National Marine Electronics Association (NMEA) messages using onboard realtime PPP processing with Trimble CenterPoint RTX for-profit service. It also logs carrier phase data for post-processing in a SD-card at 2 Hz sampling. JAVAD Delta-3 also provides realtime PPP processed data at 2.5 Hz using JAXA MADOCA data product service through QZSS LEX signals, which was a trial service and only available biweekly during our operation period. JAVAD SigmaQ has no realtime PPP function, but has attitude determination at 2.5 Hz using a four-antenna system.

A MEMS gyro (Xsens MTi-G) is also equipped to the buoy to back up attitude data. Although the absolute attitude, especially for heading, is not accurate in Xsens, it can be computed from 6-DoF outputs of tri-axial angular velocities and linear accelerations in Xsens, together with linear velocities of GPS antenna using an algorithm given by Kido et al. [41].

3.1.3. Surface Acoustic Unit

The basic function of the Surface Acoustic Unit (SAU) (Kaiyo Denshi Co., Ltd.) is transmitting a ranging signal

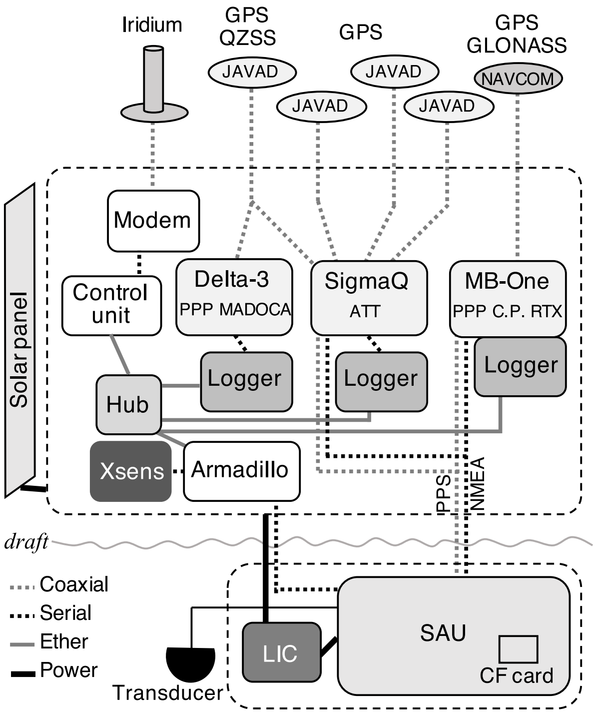

Fig. 3. A schematic illustration of the electronics on the buoy relevant to GPS-acoustic measurement. All antennae are installed on top of the buoy. GNSS receivers, data loggers, gyroscope, and control board/PCs are in a surface box denoted by the dashed square, which is surrounded by solar panels. Acoustic part, Surface Acoustic Unit (SAU) and Lithium-Ion Capacitor (LIC), is in a separate box below draft. All the electronics were commercially produced except for the loggers and control unit, which were customized for this particular system. See text for further details.

and recording ambient sound, including replied signals from the seafloor PXPs. The electric/acoustic interface for incoming and outgoing signals is a wide-directional acoustic transducer (Int'l Transducer Corp.), which is at the bottom of the buoy, $\sim$2 m below the draft. The transducer has sensitivity for 8–12 kHz signals centered at 10 kHz in frequency. The timing of transmission is exactly synchronized with the Pulse Per Second (PPS) marker given by the GPS receiver through the coaxial cable. Recording of waveform starts exactly 1 s after the transmission of the ranging signal; its time window is 10.5 s, which is long enough to cover replies from all six PXPs despite their different ranges. Raw waveform is stored in a Compact Flash (CF) card with a sampling rate of 100 kHz in a 16-bit (2 bytes) unsigned integer, which amounts to $\sim$2 MBytes ($=\sim$2 bytes$\times$100 kHz$\times$10 s) for a single ranging. Stored waveforms can be downloaded through serial communication at 115200 baud for an arbitrary window width (0–10 s) and bit-depth (1–16-bit).

For acoustic signals of precise ranging, we employed a step-sweep signal in which the frequency gradually increases from 8 to 12 kHz in 0.5 kHz steps. Each segment of constant frequency is 2 or 3 ms in length, amounting to 22 ms. Preceding this ranging signal by 1 s, the SAU transmits a 9.709 kHz burst signal of 50 ms length as a "call header." The SAU can also send a wake-up command (a coded signal of 2.2 s) to the PXPs and receives their answer to check whether they certainly woke up.

The SAU is designed to operate with 24 V electric power. Because the SAU requires a short but large electric current when transmitting a signal, its power plug is connected to a Lithium-Ion Capacitor (LIC) of 413 F ($=\sim$1.4 Ah) capacity. The consumption current of the SAU for a single ranging sequence (takes 65 s) consists of a base current (100 mA $\times$ 65 s), call header signal (16 A $\times$ 50 ms), range signal (10 A $\times$ 22 ms), optional wake-up signal (24 A $\times$ 2.4 s), and surge current to fill an internal condenser in the SAU when it is powered on (30 A $\times$ 0.2 s). These are measured values, and the durations include their transient time. In our operation, one set of measurements typically consisted of 11 successive rangings, which require only 0.08 Ah in total. The entire buoy system, including the LIC, is powered by solar panels.

An embedded Linux system controls the SAU and processes the GPS and acoustic data. The Linux system is Armadillo-420 (Atmark Techno, Inc.), in which a dedicated distribution, Atmark Dist, with an all-in-one UNIX command package "BusyBOX" runs on a 400 MHz ARM9 CPU core. The OS is installed on a nonvolatile flash memory of 16 MB, for failure-resistance. Armadillo has three serial interfaces connected to the central control unit, Xsens, and SAU, in addition to the LAN interface to record streamed NMEA messages. The typical power consumption of the Armadillo system is 1.2 W, which is shut off immediately after the measurement following analysis described in the next subsection until the next measurement begins.

3.2. Software

3.2.1. Basic Flow

A set of measurement consists of N times successive ranging with an interval at 65 s. As a basic set, we employed $N = 11$. When it is time for a regular measurement (once a week) or a command for on-demand measurement arrives from the onshore station, a measurement script starts. At the end of the script, processed data are sent back to the onshore station via satellite communication. Here, we describe each process in detail.

A series of sequential process in the script is summarized in **Fig. 4**. (1) Turn on Armadillo and Xsens. (2) Start recording Xsens data in Armadillo. (3) Turn on the LIC and SAU. (4) Send "keep alive" command to the SAU. (5) Start recording 2.5/10 Hz NMEA (antenna position and attitude) data of the GPS receivers in Armadillo. (6) Let the SAU start the measurement script (wake-up PXPs and N times of ranging) and wait for completion. (7) Receive "completed" message. (8) Stop recording Xsens and NMEA messages. (9) Send "show data header" command to the SAU. (10) Receive the data header, including NMEA positions and timestamps of all N times of transmission. (11) Compute rough synthetic traveltime

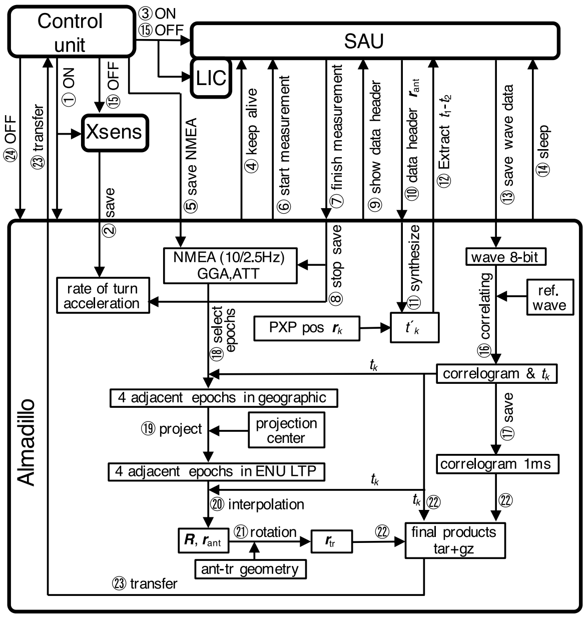

Fig. 4. A logical flow chart of onboard realtime processing of GPS-acoustic data on the buoy. The control unit conducts the procedure, which is mostly exchanges of command and data between Armadillo and Surface Acoustic Unit (SAU). For detail of the processing, especially data handling, see the text.

t'_k from antenna position $\boldsymbol{r}_{\text{ant}}(t_0)$ and k-th PXP predefined position $\boldsymbol{r}_k$. (12) Send wave extraction command to the SAU with a time window that begin at $t_1 = t'_k + \tau_{\text{delay}} - \tau_{\text{margin}}$ and end at $t_2 = t'_k + \tau_{\text{delay}} + \tau_{\text{signal}} + \tau_{\text{margin}}$ and repeat this for each PXP, where τ_{delay} is the delay line of PXP, τ_{signal} the length of ranging signal, and τ_{margin} the margin width. (13) Receive wave data from the SAU. (14) Send sleep command to the SAU. (15) Turn off the Xsens and SAU. (16) Compute cross-correlation of wave data with the reference signal to obtain exact traveltime t_k. (17) Save correlogram of 101 samples (= 1 ms) centered at t_k. (18) Extract adjacent epochs of antenna position $\boldsymbol{r}_{\text{ant}}$ and attitude $\boldsymbol{R}$ from the recorded NMEA data before and after the transmission time t_0 and reception time ${}_{\text{r}}t_k = t_0 + t_k + \tau_{\text{delay}}$, respectively. (19) Convert geographic coordinates into a local tangent plane. (20) Interpolate $\boldsymbol{r}_{\text{ant}}$ and $\boldsymbol{R}$ at time t_0 and ${}_{\text{r}}t_k$ from adjacent epochs. (21) Convert antenna position $\boldsymbol{r}_{\text{ant}}(t_0, {}_{\text{r}}t_k)$ into transducer position $\boldsymbol{r}_{\text{tr}}(t_0, {}_{\text{r}}t_k)$, using $\boldsymbol{R}(t_0, {}_{\text{r}}t_k)$ and antenna-transducer configuration data. (22) Archive and compress the relevant processed data as a final product. (23) Send the final product to the onshore station via the control unit. (24) Turn off Armadillo. These sequences are processed under a shell script and constitutive operations, such as hardware control, file I/O, and numerical computations are run with C programs, which were built from scratch.

3.2.2. Traveltime

Computation of synthetic traveltimes t'_k to determine the position of the time window for waveform extraction for each PXP is based on a rough approximation that uses simple Pythagorean distance in the Earth-Centered, Earth-Fixed (ECEF) coordinates between an antenna position in the NMEA message $\boldsymbol{r}_{\text{ant}}$ (not transducer) and a predefined position of each PXP $\boldsymbol{r}_k$ assuming a fixed uniform sound speed v, i.e., $t'_k = |\boldsymbol{r}_k - \boldsymbol{r}_{\text{ant}}|/v$. Note that the conversion of geographic into ECEF coordinates is a tiny computational burden. We consider the effect of the possible range of sound speed variation and uncertainty of the transducer position on traveltime to be smaller than 20 ms, so we append margins $\tau_{\text{margin}} = 20$ ms before and after the window to account for this uncertainty. The total length of the time window is thus a sum of signal length τ_{signal} and the two margins, i.e., $20 + 22 + 20 = 62$ ms. The procedures for calculating the wave extraction window and computation of the correlogram are summarized in **Fig. 5**.

The precise arrival time of the replied acoustic signal is defined as the time at the maximum peak in the correlogram (cross-correlation function) between the transmitted reference signal and received waveform, extracted with the time window defined above. Waveform extraction can be done with an arbitrary bit-depth, from 1 to 16-bit in our SAU. **Fig. 6(a)** shows extracted waveforms with various bit-depths, and **Fig. 6(b)** gives an enlarged view. Cases for 16-bit have been omitted because no discernible difference from the 8-bit cases can be seen. **Fig. 6(c)** shows degradation in the correlogram as a function of bit-depth. Higher bit-depth is better, but should be determined in balance with data transmission rate from the SAU to Armadillo in addition to the computational burden on Armadillo. The data transmission rate is 115200 baud. We employed 8-bit depth, which gave an adequately high-quality correlogram and the transmission time of waveform data for one set of measurement amounts to 62 ms $\times$ 100 kHz $\times$ 8 bit $\div$ 115200 baud $\times$ 6 PXPs $\times$ 11 rangings $= 28.4$ s, which is within acceptable bounds for our realtime processing.

In the correlogram computation, we employed an algorithm of simple convolution of the two signals with integer-base, because Armadillo is not equipped with Floating Point Unit (FPU). The length of convolution is 22 ms $\times$ 100 kHz $=$ 2200 samples and 8-bit integer ranges ± 128. Therefore, the temporal maximum value in the convolution can potentially be $\pm 128 \times 128 \times 2200 = 36{,}044{,}800$, which is still much smaller than the range of internal expression of 4-byte integer $\pm 2{,}147{,}483{,}648$. Employing this integer-based algorithm drastically reduces computation time to 9% of that needed by floating point-based algorithm with FPU emulation. The total time to complete the correlogram computation in Armadillo for one set of measurements is 0.85 s $\times$ 6 PXPs $\times$ 11 rangings $=$ 56.1 s.

As pointed out in Imano et al. [42], a sea surface reflection of the acoustic signal is often observed, $\sim$2 ms behind the direct path depending on draft and inclination of the buoy. In some case, reflection scores better correlation value than direct path, which results in a wrong identification of traveltime using a simple maximum correlation scheme. Our algorithm automatically identifies

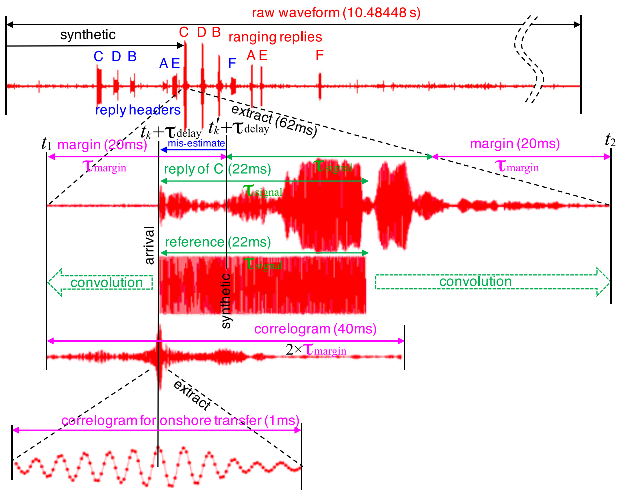

Fig. 5. Visual explanation of length and relation of an acoustic signal and correlogram. Reply signals form seafloor PXPs are recorded for 10.5 s. A target reply is extracted from this record by specifying timing based on synthetic traveltime, with a window width including adequate margins for uncertainty in the synthetic. Although the position of the maximum peak provides enough information for GPS-acoustic analysis, the waveform of the correlogram itself around the maximum peak is archived for transmission to the onshore station to further improve the analysis.

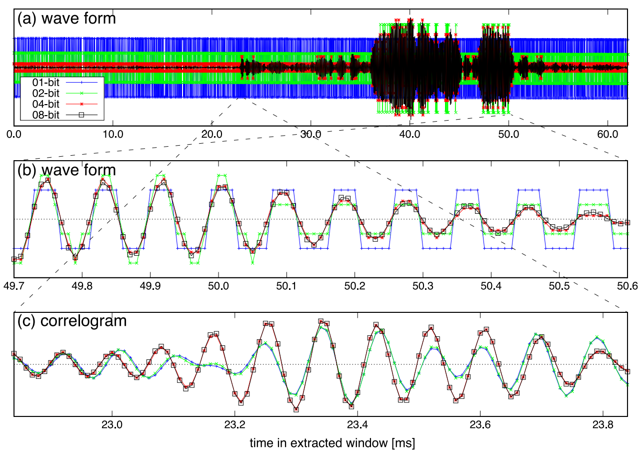

Fig. 6. Effect of bit-depth representing a raw waveform and resulting correlogram. The original 16-bit record is too fine, and no difference with 8-bit can be visually recognized. Therefore, we compared here only 1, 2, 4, and 8-bit cases. In (a) raw waveform in an extracted window and (b) its enlarged view, the effect of bit-depth directly appears its shape. However, for the resultant correlogram, a significant change in shape is observed only for 1- and 2-bit, however the timing of the maximum peak is still preserved even with the 1-bit case.

the surface reflection by recognizing if a peak larger than 60% amplitude of the maximum peak exists preceding the maximum peak by 1–3 ms. The blank of 1 ms is used to avoid picking side lobes of the original maximum peak itself.

3.2.3. Transducer Position

In addition to the exact traveltimes, the positions of the transducer at the exact timings of emission and reception of acoustic signals are needed in the GPS-A analysis. The timing of the emission is exactly synchronized with a PPS marker, and the reception is obtained based on the correlogram described above. However, realtime PPP positioning of GPS antenna and attitude based on the four-antenna system are recorded at sampling rates of 10 Hz (MB-One) or 2.5 Hz (JAVAD). Therefore, exact position or attitude at a given time must be interpolated from adjacent epochs. We employed 3rd-order Lagrange interpolation using four epochs, two before and two after the given time.

Preceding to the interpolation, positions at selected four epochs given in the geographic coordinates are converted into the East-North-Up (ENU) local tangent plane (LTP) frame using Gauss-Krüger Transverse Mercator projection (e.g., [43]) because attitude is also given as roll, pitch, and heading in the LTP-frame. The projection center is fixed at the center of the predefined PXP array, and False Easting/Northing are adjusted as the projection center is the origin of the ENU coordinates. The distortion of this LTP projection within the drifting range of the buoy ($\sim$4000 m) is smaller than 0.2 mm when compared to the nearly exact geodesic formula [44]; this amount is negligible for our purposes. Finally, the interpolated antenna position is translated into transducer position by applying frame rotation of premeasured antenna-transducer configuration with the attitude data.

3.2.4. Data Transmission

The final data product in minimal form consists of (1) time epoch of transmission, (2) transducer position at transmission in ENU coordinates, (3) a set of transducer positions at reception of the six PXPs in ENU coordinates, and (4) a set of traveltimes and correlation values for the six PXPs. These amount to 294 bytes for appropriate expression with significant digits in ASCII form. The total size of 11 rangings as a single measurement is then 3,234 bytes. After reception of these data in the laboratory via satellite communication, one can immediately calculate the horizontal array position for each of the 11 rangings and take an average if necessary. In the actual operation, the bandwidth of satellite communication allows much more data to be transmitted. Therefore, the waveform of a correlogram for $\pm$0.5 ms (= 101 bytes in 8-bit signed integer for 10 kHz sampling) for 6 PXPs $\times$ 11 rangings, data set for both MB-One and JAVAD, attitude, and other logging information are archived and compressed into a single file, which is typically 11 KB. The archived data is usually divided into $\sim$30 pieces of 340 bytes each to fit the Short Burst Data (SBD) service used in Iridium communication.

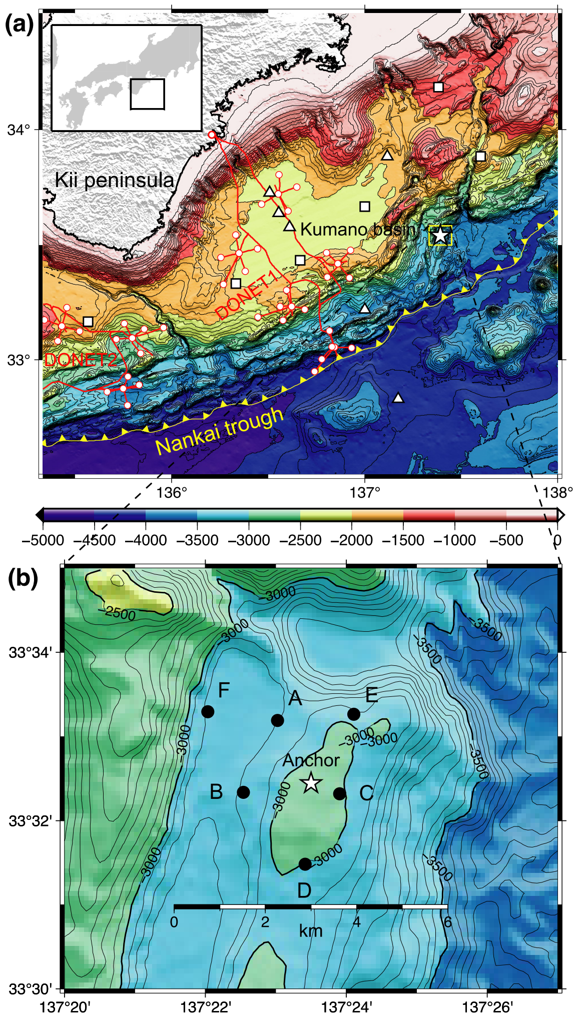

Fig. 7. (a) Regional topographic map off the Kii Peninsula, in the Nankai Trough. Contour interval is 100 m. The site of mooring operation with GPS-acoustic (GPS-A) measurements in this study is indicated by an open star. Other GPS-A sites operated by Nagoya University and Japan Coast Guard are plotted for comparison by open triangles and squares, respectively. DONET1 and part of DONET2 seafloor cables are drawn with red lines. The trough axis is drawn by a yellow line with triangles. (b) Enlarged view of the mooring site indicated by yellow open box in (a). Position of the anchor and the six seafloor PXPs with their IDs for GPS-A measurements are plotted by open star and solid circles, respectively. Contour interval is 50 m.

4. Operation and Result

4.1. Site Description

The GPS-A site used in this research was constructed on the trench side slope (~3000 m in depth) of the outer ridge of the Kumano Basin, off the Kii Peninsula along the Nankai Trough, as shown in **Fig. 7(a)**. Six PXPs were installed, rather than the traditional three or four, for the countermeasure against a largely drifting buoy and to enable the possibility of evaluating the horizontal sound speed gradient associated with the Kuroshio Current. This geographic site was selected for following reasons. (1) The site is located in the expected source region of the To-Nankai earthquake and between the trough axis and surface trace of the splay fault, where one can effectively distinguish which plane is ruptured (decollement or mega-splay fault). (2) The site is often passed over by the strong Kuroshio Current, which allowed us to examine the robustness of our system and evaluate the accuracy of the GPS-A measurements in such adverse sea conditions; the buoy experienced a current over 5 knots during the trials. (3) The site is complementary in location to other GPS-A sites constructed by Nagoya University and Japan Coast Guard. It is utilized not only as realtime monitoring but also as a traditional campaign site to investigate plate coupling. (4) The site is far enough away from existing seafloor cables (including undisclosed ones) for safety and is on a single terrace, allowing the PXP array to be rigid without internal deformation (**Fig. 7(b)**).

The site was constructed in 2012 with six hybrid-type PXPs designed to work both with Tohoku University and Nagoya University systems. Since then, traditional campaign-style surveys have been repeatedly conducted by Nagoya University, mainly for investigation of plate coupling condition, and by Tohoku University, mainly for precise determination of relative position among the six PXPs for accurate realtime monitoring with a buoy observation addressed in the discussion.

4.2. Mooring Operation

In the past, we developed a prototype buoy system and conducted experimental mooring operations. The first operation lasted for four months, starting in Dec. 2012, and the second one had a duration of five months, starting in Jan. 2014. The whole buoy system has a number of elements being developed, however, we focus here on GPS-A measurement. In the first operation, acoustic ranging itself functioned properly through the operational period, although storing full GPS data failed due to a hardware problem. In the second operation, both regular and on-demand measurements worked successfully, and data storing was also succeeded. However, not all onboard realtime data processing had yet been implemented. Only acoustic waveforms were automatically clipped, and its correlogram was transmitted to the onshore station via satellite communication. Therefore, seafloor position data were obtained by post-processing GPS data after recovering the buoy. However, we obtained enough data to design a deliberate algorithm to perform realtime data processing especially for exceptional handling against unexpected data. The third, most recent, operation lasted for over a year, from Dec. 2015 until Dec. 2016. The basic specifications of the buoy are described in Takahashi et al. [38] and details of the operation are reported in Fukuda et al. [45].

Figure 8(a) shows the location of the buoy across the whole mooring period at hourly intervals to enable visual perception of the existence of the buoy like a probability density function. It is noticeable that the buoy was on a circumference of 3600–4000 m radius during most

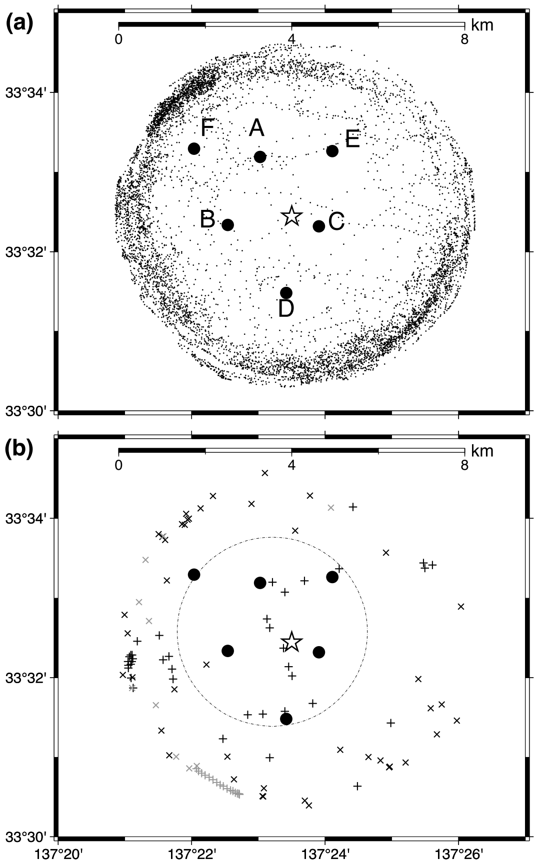

Fig. 8. (a) Tracking chart of the buoy during the entire period of the one-year mooring operation. Position was plotted every one hour, indicated by small dots. The buoy tends to be on the circumference of a circle of 3.6–4.0 km radius with its center at the anchor (indicated by an open star). The solid circles indicate six PXPs with their IDs. (b) Position of the buoy at regular (weekly) and on-demand measurements, indicated by "×" and "+," respectively. Gray symbols denote serial ranging numbers ≥1000, which failed to transmit data due to a bug in the script (offline data is available). The dotted circle indicates a 2.2 km radius from the array center (not the anchor), used to separate the areas "inside" and "outside" of the array in this study.

of the period. The radius of 3600 m corresponds to the nominal range of the slack ratio 1.57 with relatively weak current, while the 4000 m indicates the mooring cable is tense and resiliently stretched due to strong current. In **Fig. 8(b)**, positions at regular and on-demand measurements are plotted by "×" and "+," respectively. The dotted circle indicates a 2.2 km radius from the array center (not from the anchor), which classifies the measurement positions into inside/outside of the array in the later section. A regular measurement consisting of 11 successive rangings at intervals of 65 s was conducted at 15:00 (JST) every Monday afternoon, amounting to 53 times across the total period. On-demand measurements, also consisting of 11 rangings, were only carried out when an order from the onshore station was received. Although the on-demand measurements are supposed to take immediately after a large earthquake in actual operation, they were conducted when the buoy happened to come closer to the center in order to collect data with various geometrical situations other than from the circumference in this trial-based operation. A total of 55 on-demand measurements were made, including intensive on-demand measurements conducted concurrently with a ship-based campaign survey just before recovering the buoy.

4.3. GPS-A Data

Transmitted data of each GPS-A measurement through Iridium SBD parted messages were reassembled into a single archive and unpacked to be readable files. All the required data for GPS-A, i.e., epoch, traveltimes, and transducer positions at the timing of transmission and reception, were included, as well with other auxiliary information. With these data, PXP array positions can be instantly calculated through the algorithm introduced in Kido et al. [21]. All array positions obtained through the yearlong operation are plotted in **Fig. 9(a)** with respect to the predefined position. Solid circles represent data recorded when the buoy was within 2.2 km from the array center (regarded as "inside the array" indicated by a dotted circle in **Fig. 8(b)**), while open circles indicate that the buoy was outside this range. Note that array positions are included only when all six replies were properly identified. Since our current goal of accuracy is much larger than the secular motion of this area, namely ∼4 cm/yr [33], we evaluated the accuracy of our data simply as a deviation from the origin. Significant degradation in accuracy (∼1.0 m in 2σ, indicated by the outer circle) was observed outside the circle, although it still achieved the initial goal of the SIP project, i.e., detecting displacement associated with a M8-class earthquake. Inside the array, indicated by the inner circle, the accuracy improved to ∼46 cm (2σ), which is comparable with repeatability of a single ranging in campaign-style surveys, which are often largely affected by lateral sound speed variation if a temporal average is not taken. **Fig. 9(b)** shows all slant acoustic paths to the six PXPs for the plots in **Fig. 9(a)** in the viewpoint of the buoy. The black lines are the paths when the buoy was inside the array, while the gray lines are when it was outside. The longest path reaches 6500 m in the horizontal distance (7200 m in the slant distance) with a nadir angle of 64.5°.

The gray symbols in **Fig. 8(b)** are the positions where measurements were taken, for which realtime processing failed. All the measurements with a sequential ranging number ≥1000 encountered this problem because of a bug in the script that limited the ranging number to only 3 digits. On-demand measurements were much more frequent than initially expected; the total number exceeded 1000 on Oct. 3, 2016. From then until recovery of the buoy on Dec. 20, 2016 (ranging numbers 1000–1303), realtime processing was missing and only offline data were available after recovering the buoy. Only realtime data were plotted in **Fig. 9** and analysis including the offline data will be considered in the future. Note that the 17 aligned gray crosses southwest of the array in **Fig. 8(b)** are mea-

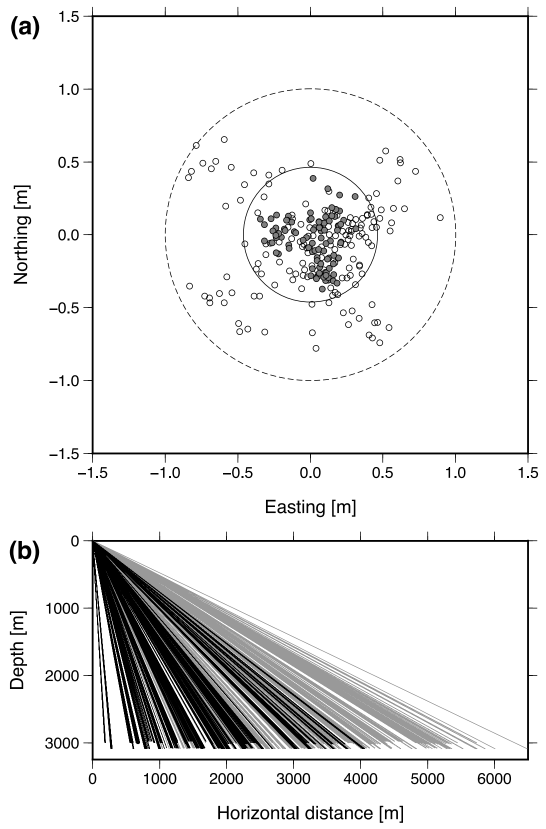

Fig. 9. (a) Apparent array positions obtained through the one-year mooring operation. Solid circles indicate data obtained when the buoy was within a 2.2 km horizontal distance from the array center, while open circles were used when the buoy was outside this limit. Note that the array positions are plotted only when all six replies from the PXPs were properly identified. (b) Slant acoustic paths to the six PXPs for the plot in (a), in a viewpoint from the buoy. Black lines are the paths when the buoy was inside the array, while the gray lines were used when the buoy was outside the array. The most distant path is 6500 m in the horizontal distance (7200 m in the slant range) corresponding to 64.5° of nadir angle.

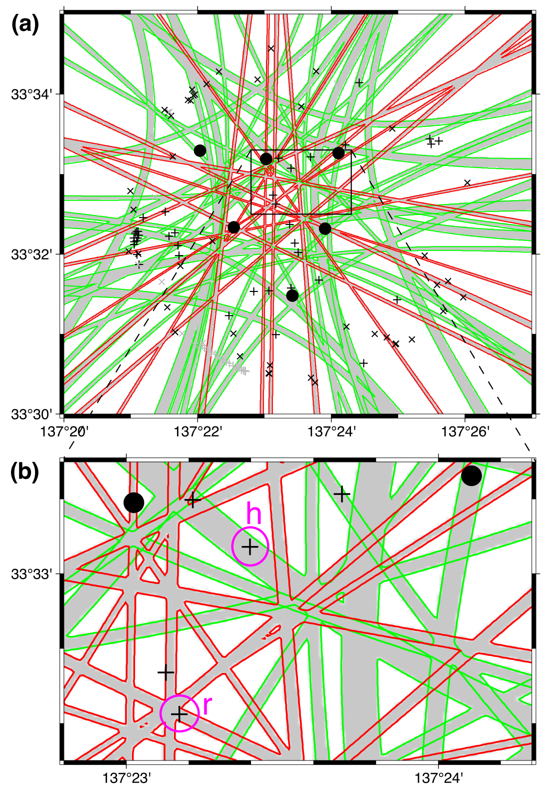

Fig. 10. (a) Zones of buoy position, where a replied ranging signal of one PXP overlaps with a ranging signal (red) or a reply header signal (green) of another PXP. Each zone has its own finite width related to signal length (22 ms for ranging and 50 ms for reply header) and visual angle of separation of the two PXPs. Positions of the PXPs and measurements during the operation (same as in **Fig. 8**) are superimposed. (b) Enlarged view of the area indicated by a rectangle in (a). Positions labeled "h" and "r" are examples of "range-header" and "range-range" overlaps shown in **Figs. 11** and **12**.

surements taken concurrently with a campaign survey using a research vessel just before recovery of the buoy. Simultaneous measurements from two different surface positions may give information on lateral sound speed variation; this is a subject to investigate in a separate paper.

In addition to the offline data above, a notable fraction of the data is not plotted in **Fig. 9**. This is because the array position was plotted only when all six PXPs responded. A portion of the cases in which not all PXPs responded is just failure of automatic pickup of the traveltime due to overlapping multiple replies. This is addressed in the discussion section.

5. Discussion

5.1. Overlap of Replied Acoustic Signals

The PXPs installed at this site can respond either separately or all together. We set the PXPs to the latter mode, so that measurement time and thus power consumption was reduced to $1/6$ of the former mode. However, reply signals from different PXPs can have a chance to overlap in timing, which may degrade the signal quality. Each pair of PXPs has its own overlap buoy position, where distances to both PXPs are equal. Zone width D depends on the signal length and separation angle of a PXP pair as $D = v \cdot \tau_{\mathrm{signal}} / \sin(\theta/2)$, where v is mean sound speed, τ_{signal} the signal length, and θ the visual angle between the two PXPs from the buoy. For our array geometry of six PXPs, the number of zones is ${}_6C_2 = 15$, which are shown by red zones in **Fig. 10**. In addition to this "range-range" combination, our PXP has a reply header signal to be counted for overlap with the ranging signal, "range-header" and "header-range," which amount to ${}_6P_2 = 30$ combinations as shown by green zones in **Fig. 10**. Because the reply header arrives 1 s prior to the ranging signal, the shape of the resulting zone is hyperbolic, an intersection of hyperboloid with sea surface plane, while the range-range overlap zone is linear.

We can set an arbitrary delay to each PXP by send-

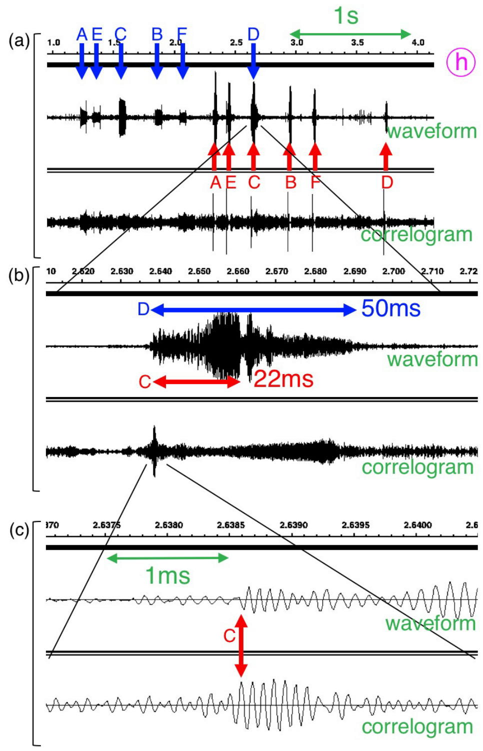

Fig. 11. (a) Main part of the raw waveform at the position labeled "h" in **Fig. 10**, an example of overlap reply header of PXP-D and reply ranging signal of PXP-C. (b) Enlarged view of the signal part. (c) Further enlargement around the correlation peak. No significant degradation in the correlogram due to the overlap is observed.

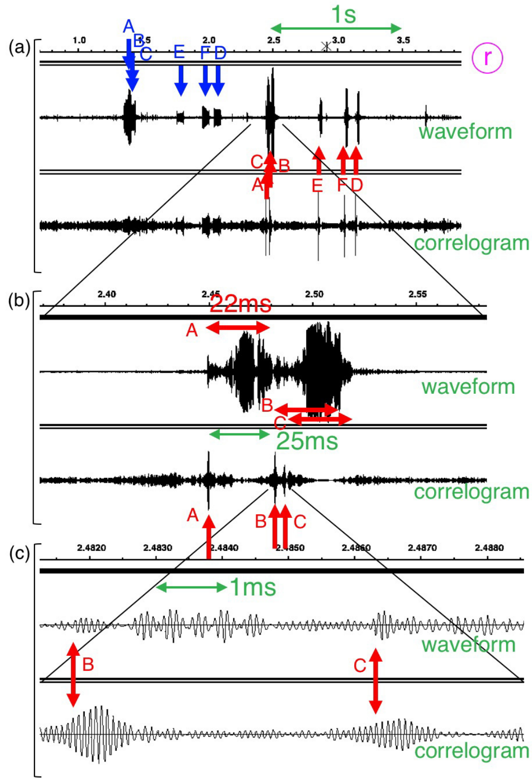

Fig. 12. Same as **Fig. 11**, but for the position labeled "r" in **Fig. 10**, an example of overlap between the reply ranging signals to each other (PXP-B and PXP-C). The first peak in the correlogram for PXP-B remains unchanged, however, the second peak shows smaller value.

ing an acoustic command beforehand so that the overlap zone changes its position accordingly. This is quite effective in fixed-point surveys to keep the overlap zones away from the center of the array, although the selection of the delay amount is somewhat puzzled with six PXPs. On the contrary, a delay does not make sense for moored buoy measurements because the buoy changes its position with time. Therefore, we did not set a delay to any PXP in the mooring operation. As can be seen in **Fig. 10**, overlap zones covered at least one-third of the area over the array. The effect of the overlapping of raw waveform on correlogram for traveltime detection must therefore be examined. **Fig. 11** gives an example of raw waveform obtained at the buoy position labeled "h" in **Fig. 10(b)**, where the ranging reply of PXP-C was expected to overlap with the replied header of PXP-D. As expected by synthetic traveltimes, the ranging data (red arrow) entirely overlapped with the reply header signal of comparable amplitude (blue arrow) in the recorded raw waveform. However, owing to the non-correlative nature of phase modulated signals with others, the correlogram was not notably degraded. It should be noted that the multiple follow-on sidelobes are not due to the overlap, but rather caused by characteristics of our PXPs, and that the second major peak represents the true arrival [46].

We will now discuss ranging-ranging overlap. The data shown in **Fig. 12** are taken from the position labeled "r" in **Fig. 10(b)**, where three ranging replies from PXP-A, B, and C are close to each other. Even though the replies from PXP-B and C almost fully overlap, the correlogram can still distinguish the two arrivals. However, the peak for PXP-C in the correlogram is small and degraded. Besides, if the two peaks were closer than 20 ms (the margin time for uncertainty in auto-detection), the two peaks would appear in the same window and the larger peak would be counted for both PXPs. To avoid this, one must employ a narrower margin using a precise synthetic traveltime, accounting for transducer position and sound speed variation, or introducing a more complicated algorithm that accounts for trends in traveltime changes among successive measurements.

5.2. Degradation of Accuracy at Outside the Array

Because realtime positioning is intrinsically equivalent to point survey from an arbitrary position, degradation of accuracy as a function of buoy position is crucial. This can be primarily investigated using "condition number," or geometrical strength of inverse problem [37]. While Kido [37] discussed lateral sound speed gradient, in this study we consider only stratified structure to focus on the buoy-specific observation. First, we investigate the condition number for the case of three PXPs, shown in **Fig. 13**.

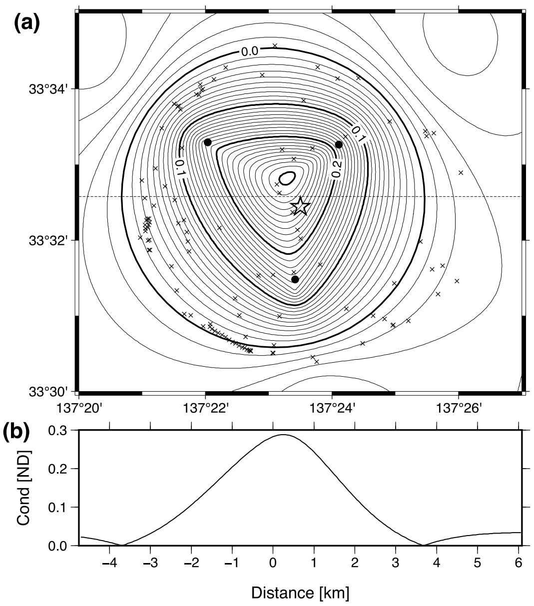

Fig. 13. (a) Condition number as a function of survey position, representing the geometrical strength to solve array position from a single ranging. A case of three PXPs (by removing the three internal PXPs from our site) is shown. The interval of the thick contour is 0.1 (non-dimensional). Our buoy positions (slack ratio: 1.57) are shown for comparison. (b) Cross section of condition number along the EW line indicated in (a). A ring-like singular zone (condition number is zero) of ∼3.7 km radius appears, where the condition is mathematically indeterminate.

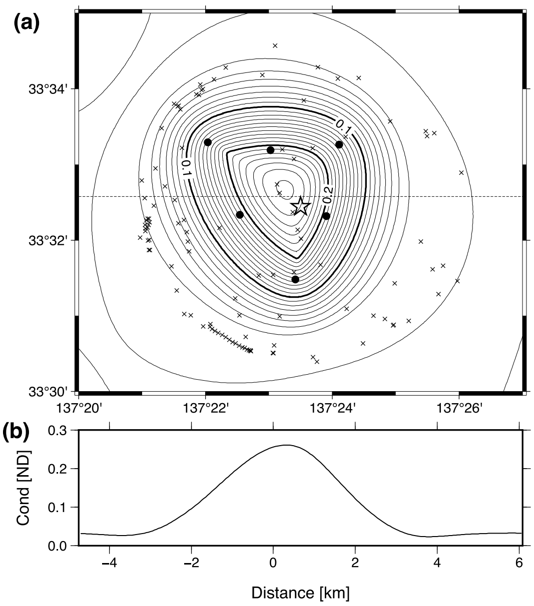

Fig. 14. The same as **Fig. 13**, but for six PXPs, the case of our site. The singular ring no longer exists, however, the condition is still poor for outside the array, where the accuracy of array positioning is degraded.

The ideal position is the center of the array, as expected. However, it can clearly be seen that a singular zone, or condition number of zero, surrounds the array. In this singular zone, changes in sound speed and in horizontal array position have mathematically equivalent effect on traveltime. This means the two variables become indistinguishable, rendering the problem indefinite. If three additional PXPs are installed inside the existing triangle (as is the case at our site), the singular zone vanishes, as shown in **Fig. 14**, although the area outside the array is still in an ill-condition. This is the primary reason of degradation of accuracy outside the array.

The other cause of degradation is the buoy drifting due to sea current. An advantage of the GPS-A point survey is that the effect of uncertainty in the predefined array geometry (relative position among the PXPs) on the array positioning remains constant as long as the survey position does not change (not necessary at the array center). This means that any error originating from array geometry will be fully canceled in array displacement. However, the buoy is drifting and this advantage cannot be in effect, especially in the case of large drift outside the array. One must determine the array geometry as precisely as possible by campaign survey beforehand. The predefined array geometry in this study was determined with an algorithm [47] customized for moving survey. Details of characteristics of uncertainty in array geometry for buoy-based surveys and error propagation are investigated in Imano et al. [48].

If a buoy-based GPS-A survey is carried out using only three PXPs, the buoy must be tautly moored so that the drift range does not extend to the singular zone outside the array. However, taut mooring is difficult in regions with strong current. In this context, improvement of the Drag Coefficient (C_d) of the buoy and mooring cable is crucial to minimize the slack ratio. The slack ratio of our current buoy system is 1.57, allowing drift of 3600–4000 m, including stretching, for 3000 m depth and 5.5 knot current. This still results in a poor condition number, even with six PXPs (**Fig. 14**). If the slack ratio can be reduced to 1.2–1.3, the drift range drops to 2000–2500 m, which greatly improves the condition number.

An alternative approach is to construct a larger triangle array of PXPs; a triangle with a significantly larger dimension compared to its depth results in a larger area of improved condition number, covering the drifting range of the buoy. However, the distance from the buoy to the PXP on the opposite side is becoming too large, in the sense that the nadir angle is getting too close to 90°, which may result in missing acoustic communications. Note that the largest nadir angle is already as large as 64.5° with the current array geometry as shown in the **Fig. 9(b)**.

5.3. Areas for Improvement

The algorithm of GPS-A point survey analysis [21] assumes the survey position is at the center of the array so that sound speed change and any vertical motion do not affect the estimate of horizontal motion. However, when the survey position deviates from the array center, vertical motion significantly affects apparent horizontal mo-

Table 2. Comparison of surface platforms in realtime seafloor geodetic monitoring.

Surface platform	Ship	Cable	Buoy	ASV	Wave Glider
Horizontal	○	×	○	○	○
Vertical	○	×	○	△	△
Realtime (endurance)	×	○	○	△	○
Moving	○	N/A	×	△	×
Sea current	○	○	○	△	×
Sea state	×	○	○	○	○
Fishery	○	○	×	△	△
Portability	○	×	△	○	○
Cost (USD)	10k/day∼	100,000k∼	1,000k∼	2,000k∼	300k∼

tion. Realtime positioning, and thus, point survey, intrinsically cannot solve vertical motion when sound speed is unknown, as in the case of buoy-based surveys. Therefore, the vertical motion must be monitored with independent observation and reflected to the predefined array position. Fortunately, our buoy system measures both sea surface height and bottom pressure, which is acoustically transferred to the buoy via WES [49, 50], so that vertical motion can be immediately separated from the change in sea surface height due to a tsunami. Therefore, we can properly measure horizontal motion by applying vertical movement thus obtained to the predefined array position. This procedure is important and should be implemented as an automatic sequence in any practical operation.

As shown in **Fig. 10**, overlap zones of multiple acoustic signals occupy a significant fraction of the area, although superposition of reply header is not critical for arrival detection in the correlogram. The reply header signal is a legacy function, which is not actually used in the current analysis. Eliminating the reply header function of a PXP can reduce overlap zones and also has the advantage of reducing the power consumption of the PXP. The reply header length (50 ms) is much longer than that of a ranging signal (22 ms), so this step has a remarkable energy-saving effect. In addition, a reply message in response to a wake-up signal is up to 2.2 s; this can be also eliminated. Power for the SAU side is supplied by solar panels, and much more frequent measurements are possible, even in the current system. However, the current PXPs are designed for campaign-style surveys and work with an internal battery of finite capacity. This is the reason regular measurements were only taken weekly in our mooring operation. If we were to employ PXPs customized for a mooring operation with unnecessary reply header and messages eliminated, regular measurements could be carried out daily, giving nearly continuous data.

5.4. Pros and Cons of Moored Buoy-Based Observation

When considering realtime monitoring of seafloor movement, the choice of a surface platform highly depends on the conditions, which are briefly summarized in **Table 2**. In a region with strong current, like the Pacific side of Japan, only a slackly moored buoy can be employed. A Wave Glider can be controlled only up to 1–2 knots at most. ASV can manage conditions up to 3 knost, however, its endurance is several months. This illustrates that a Wave Glider is too slow to conduct a moving survey. Vertical seafloor movement is measured by OBP when using a buoy, while purely GPS-A is assumed for a ship, ASV, and Wave Glider. A buoy, ASV, and Wave Glider can withstand stormy sea conditions. The most delicate problem is fishery activity; the mooring wire of a buoy sometimes interferes even with subsurface longline fishery nets, while an ASV or Wave Glider can pass through the net. Although the mooring cable can withstand this interference, it is advisable to consult with the relevant fishery association beforehand. In terms of fiscal cost, operating a buoy is much more efficient than using a seafloor cable, although the cable system intrinsically contains many observation sites. This is because a buoy can be reinstalled at different sites on-demand, whereas a cable is usually installed permanently.

Acknowledgements

We thank the anonymous reviewers and editor for their helpful comments about how to improve the manuscript. This research was supported by JST under the cross-ministerial Strategic Innovation Promotion Program (SIP) "Enhancement of Societal Resiliency against Natural Disasters" through the 2014–2016 fiscal years. The six PXPs used in this study and the prototype of the buoy were initially constructed in 2012, under the MEXT project for "Development of GPS/Acoustic Technique." This research is part of the MEXT/JSPS "Research project for compound disaster mitigation on the great earthquakes and tsunamis around the Nankai Trough region" and KAKENHI Grant Number 17K18799. We thank the crew members and MWJ technicians in R/V Kaiyo and Yokosuka for installing and recovering the buoy.

References:

[1] Y. Kaneda, K. Hirahara, and T. Furumura, "New Research Project for Evaluating Seismic Linkage Around the Nankai Trough –Integration of Observation, Simulation, and Disaster Mitigation–," J. Disaster Res., Vol.4, No.2, pp. 61-66, doi:10.20965/jdr.2009.p0061, 2009.

[2] T. Hori, "Earthquake and Tsunami Scenarios as Basic Information to Prepare Next Nankai Megathrust Earthquakes," J. Disaster Res., Vol.12, No.4, pp. 775-781, doi:10.20965/jdr.2017.p0775, 2017.

[3] Y. Kaneda, "Resilience Science for a Resilience Society in Seismogenic and Tsunamigenic Countries," J. Disaster Res., Vol.12, No.4, pp. 712-721, doi:10.20965/jdr.2017.p0712, 2017.

[4] T. Kato, Y. Terada, M. Kinoshita, H. Kakimoto, H. Isshiki, M. Matsuishi, A. Yokoyama, and T. Tanno, "Real-time observation of tsunami by RTK-GPS," Earth Planets Space, Vol.52, pp. 841-845, doi:10.1186/BF03352292, 2000.

[5] T. Nagai, "Development and Improvement of the Nationwide Coastal Wave Observation Network," Proc. Techno-Ocean'2002, Paper-T1-1-2, 4pp., 2002.

[6] Y. Terada, T. Kato, T. Nagai, S. Koshimura, N. Imada, H. Sakaue, and K. Tadokoro, "Recent Developments of GPS Tsunami Meter

for a Far Offshore Observations," GENAH, IAG Symp., Vol.145, pp. 145-153, doi:10.1007/1345_2015_151, 2015.

[7] L. Mervart, Z. Lukes, C. Rocken, and T. Iwabuchi, "Precise point positioning with ambiguity resolution in real-time," Proc. of the 21st Int. Technical Meeting of the Satellite Division of The Institute of Navigation (ION GNSS 2008), pp. 397-405, 2008.

[8] R. Hino, D. Inazu, Y. Ohta, Y. Ito, S. Suzuki, T. Iinuma, Y. Osada, M. Kido, H. Fujimoto, and Y. Kaneda, "Was the 2011 Tohoku-Oki earthquake preceded by aseismic preslip? Examination of seafloor vertical deformation data near the epicenter," Mar. Geophys. Res., Vol.35, pp. 181-190, doi:10.1007/s11001-013-9208-2, 2014.

[9] K. Kawaguchi, Y. Kaneda, and E. Araki, "The DONET: A real-time seafloor research infrastructure for the precise earthquake and tsunami monitoring," Proc. of OCEANS'08 MTS/IEEE KOBE-TECHNO-OCEAN'08, doi:10.1109/OCEANSKOBE.2008.4530918, 2008.

[10] Y. Kaneda, K. Kawaguchi, E. Araki, H. Matsumoto, T. Nakamura, S. Kamiya, K. Ariyoshi, T. Hori, T. Baba, and N. Takahashi, "Development and application of an advanced ocean floor network system for megathrust earthquakes and tsunamis, Seafloor Observatories," P. Favali et al., Springer Praxis Books, doi:10.1007/978-3-642-11374-1_25, pp. 643-662, 2015.

[11] N. Takahashi, K. Imai, M. Ishihara, K. Sueki, R. Obayashi, T. Tanabe, F. Tamazawa, T. Baba, and Y. Kaneda, "Real-Time Tsunami Prediction System Using DONET," J. Disaster Res., Vol.12, No.4, pp. 766-774, doi:10.20965/jdr.2017.p0766, 2017.

[12] K. Uehira, T. Kanazawa, S. Noguchi, S. Aoi, T. Kunugi, T. Matsumoto, Y. Okada, S. Sekiguchi, K. Shiomi, M. Shinohara, and T. Yamada, "Ocean bottom seismic and tsunami network along the Japan Trench," 2012 AGU Fall Meeting abstract OS41C-1736, 2012.

[13] F. I. González, H. M. Milburn, E. N. Bernard and J. C. Newman, "Deep-ocean Assessment and Reporting of Tsunamis (DART): Brief Overview and Status Report." Proc. of the Int. Workshop on Tsunami Disaster Mitigation, 1998.

[14] H. Tsushima, R. Hino, H. Fujimoto, Y. Tanioka, and F. Imamura, "Near-field tsunami forecasting from cabled ocean bottom pressure data," J. Geophys. Res., Vol.114, B06309, doi:10.1029/2008JB005988, 2009.

[15] Y. Ohta, T. Kobayashi, H. Tsushima, S. Miura, R. Hino, T. Takasu, H. Fujimoto, T. Iinuma, K. Tachibana, T. Demachi, T. Sato, M. Ohzono, and N. Umino, "Quasi real-time fault model estimation for near-field tsunami forecasting based on RTK-GPS analysis: Application to the 2011 Tohoku-Oki earthquake (Mw 9.0)," J. Geophys. Res., Vol.117, doi:10.1029/2011JB008750, 2012.

[16] H. Tsushima, R. Hino, Y. Ohta, T. Iinuma, and S. Miura, "tFISH/RAPiD: Rapid improvement of near-field tsunami forecasting based on offshore tsunami data by incorporating onshore GNSS data," Geophys. Res. Lett., Vol.41, pp. 3390-3397, doi:10.1002/2014GL059863, 2014.

[17] H. Tsushima and Y. Ohta, "Review on near-field tsunami forecasting from offshore tsunami data and onshore GNSS data for tsunami early warning," J. Disaster Res., Vol.9, No.3, pp. 339-357, doi:10.20965/jdr.2014.p0339, 2014.

[18] F. N. Spiess, "Suboceanic geodetic measurements," IEEE Trans. on Geoscience and Remote Senssing, GR-23, pp. 502-510, doi:10.1109/TGRS.1985.289441, 1985.

[19] F. N. Spiess, C. D. Chadwell, J. A. Hildebrand, L. E. Young, G. H. Purcell Jr., and H. Dragert, "Precise GPS/acoustic positioning of seafloor reference points for tectonic studies," Phys. Earth Planet. Inter., Vol.108, No.2, pp. 101-112, doi:10.1016/S0031-9201(98)00089-2, 1998.

[20] K. Tadokoro, M. Ando, R. Ikuta, T. Okuda, G. Besana, S. Sugimoto, and M. Kuno, "Observation of coseismic seafloor crustal deformation due to M7 class offshore earthquakes," Geophys. Res. Lett., Vol.33, L23306, doi:10.1029/2006GL026742, 2006.

[21] M. Kido, H. Fujimoto, S. Miura, Y. Osada, K. Tsuka, and T. Tabei, "Seafloor displacement at Kumano-nada caused by the 2004 off Kii Peninsula earthquakes, detected through repeated GPS/Acoustic surveys," Earth Planets Space, Vol.58, pp.911-915, doi:10.1186/BF03351996, 2006.

[22] M. Fujita, T. Ishikawa, M. Mochizuki, M. Sato, S. Toyama, M. Katayama, K. Kawai, Y. Matsumoto, T. Yabuki, A. Asada, and O. L. Colombo, "GPS/Acoustic seafloor geodetic observation: method of data analysis and its application," Earth Planets Space, Vol.58, pp.265-275, doi:10.1186/BF03351923, 2006.

[23] Y. Matsumoto, M. Fujita, T. Ishikawa, M. Mochizuki, T. Yabuki, and A. Asada, "Undersea co-seismic crustal movements associated with the 2005 Off Miyagi Prefecture Earthquake detected by GPS/acoustic seafloor geodetic observation," Earth Planets Space, Vol.58, pp. 1573-1576, doi:10.1186/BF03352663, 2006.

[24] M. Sato, H. Saito, T. Ishikawa, Y. Matsumoto, M. Fujita, M. Mochizuki, and A. Asada, "Restoration of interplate locking after the 2005 Off-Miyagi Prefecture earthquake, detected by GPS/acoustic seafloor geodetic observation," Geophys. Res. Lett., Vol.38, L01312, doi:10.1029/2010GL045689, 2011.

[25] M. Sato, M. Fujita, Y. Matsumoto, T. Ishikawa, H. Saito, M. Mochizuki, and A. Asada, "Interplate coupling off northeastern Japan before the 2011 Tohoku-oki earthquake, inferred from seafloor geodetic data," J. Geophys. Res. Solid Earth, Vol.118, No.7, pp. 3860-3869, doi:10.1002/jgrb.50275, 2013.

[26] M. Sato, T. Ishikawa, N. Ujihara, S. Yoshida, M. Fujita, M. Mochizuki, and A. Asada, "Displacement above the hypocenter of the 2011 Tohoku-oki earthquake," Science, Vol.332, pp. 1395, doi:10.1126/science.1207401, 2011.

[27] M. Kido, Y. Osada, H. Fujimoto, R. Hino, and Y. Ito, "Trench-normal variation in observed seafloor displacements associated with the 2011 Tohoku-Oki earthquake," Geophys. Res. Lett., Vol.38, L24303, doi:10.1029/2011GL050057, 2011.

[28] S. Watanabe, M. Sato, M. Fujita, T. Ishikawa, Y. Yokota, N. Ujihara, and A. Asada, "Evidence of viscoelastic deformation following the 2011 Tohoku-Oki earthquake revealed from seafloor geodetic observation," Geophys. Res. Lett., Vol.41, pp. 5789-5796, doi:10.1002/2014GL061134, 2014.

[29] T. Sun, W. Kelin, T. Iinuma, R. Hino, J. He, H. Fujimoto, M. Kido, and Y. Osada, "Prevalence of viscoelastic relaxation after the 2011 Tohoku-oki earthquake," Nature, Vol.514, pp. 84-87, doi:10.1038/nature13778, 2014.

[30] F. Tomita, M. Kido, Y. Ohta, T. Iinuma, and R. Hino, "Along-trench variation in seafloor displacements after the 2011 Tohoku earthquake," Science Advances, Vol.3, No.7, e1700113, doi:10.1126/sciadv.1700113, 2017.

[31] K. Tadokoro, R. Ikuta, T. Watanabe, M. Ando, T. Okuda, S. Nagai, K. Yasuda, and T. Sakata, "Interseismic seafloor crustal deformation immediately above the source region of anticipated megathrust earthquake along the Nankai Trough, Japan," Geophys. Res. Lett., Vol.39, L10306, doi:10.1029/2012GL051696, 2012.

[32] Y. Yokota, T. Ishikawa, S. Watanabe, T. Tashiro, and A. Asada, "Seafloor geodetic constraints on interplate coupling of the Nankai Trough megathrust zone," Nature, Vol.534, pp. 374-377, doi:10.1038/nature17632, 2016.

[33] K. Yasuda, K. Tadokoro, S. Taniguchi, H. Kimura, and K. Matsuhiro, "Interplate locking condition derived from seafloor geodetic observation in the shallowest subduction segment at the Central Nankai Trough, Japan," Geophys. Res. Lett., Vo.44, pp. 3572-3579, doi:10.1002/2017GL072918, 2017.

[34] M. Kido, H. Fujimoto, R. Hino, Y. Ohta, Y. Osada, T. Iinuma, R. Azuma, I. Wada, S. Miura, S. Suzuki, F. Tomita, and M. Imano, "Progress in the Project for Development of GPS/Acoustic Technique Over the Last 4 Years," GENAH, IAG Symp., Vol.145, pp. 3-10, doi:10.1007/1345_2015_127, 2015.

[35] C. D. Chadwell, "GPS-Acoustic Seafloor Geodesy using a Wave Glider," AGU Fall Meeting, abstract G14A-01, 2013.

[36] M. Kido, Y. Osada, and H. Fujimoto, "Temporal variation of sound speed in ocean: a comparison between GPS/acoustic and in situ measurements," Earth Planet Space, Vol.60, pp. 229-234, doi:10.1186/BF03352785, 2008.

[37] M. Kido, "Detecting horizontal gradient of sound speed in ocean," Earth Planet Space, Vol.59, e33-e36, doi:10.1186/BF03352027, 2007.

[38] N. Takahashi, Y. Ishihara, H. Ochi, T. Fukuda, J. Tahara, Y. Maeda, M. Kido, Y. Ohta, K. Mutoh, G. Hashimoto, S. Kogure, and Y. Kaneda, "New buoy observation system for tsunami and crustal deformation," Mar. Geophys. Res., Vol.35, pp. 243-253, doi:10.1007/s11001-014-9235-7, 2014.

[39] N. Takahashi, Y. Ishihara, T. Fukuda, H. Ochi, J. Harada, T. Mori, M. Deguchi, M. Kido, Y. Ohta, R. Hino, K. Mutoh, G. Hashimoto, O. Motohashi, and Y. Kaneda, "Buoy Platform Development for Observation of Tsunami and Crustal Deformation," GENAH, IAG Symp., Vol.145, pp. 97-103, doi:10.1007/1345_2015_114, 2015.

[40] N. Takahashi, K. Imai, Y. Ishihara, T. Fukuda, H. Ochi, K. Suzuki, M. Kido, Y. Ohta, M. Imano, and R. Hino, "Real-time and on-demand buoy observation system for tsunami and crustal displacement," AGU Fall Meeting, abstract NH23A-0220, 2017.

[41] M. Kido, H. Fujimoto, and Y. Osada, "Utilizing motion sensor data in past seafloor geodetic measurements," J. Geodetic Soc. Japan, Vol.54, pp. 163-179, doi:10.11366/sokuchi1954.54.163, 2008 (in Japanese with English abstract).

[42] M. Imano, M. Kido, Y. Ohta, T. Fukuda, H. Ochi, N. Takahashi, and R. Hino, "Improvement in the Accuracy of Real-time GPS/Acoustic Measurements Using a Multi-purpose Moored Buoy System by Removal of Acoustic Multipath," GENAH, IAG Symp., Vol.145, pp. 105-114, doi:10.1007/1345_2015_192, 2015.

[43] International Association of Oil and Gas Producers (IOGP), "Coordinate Conversions and Transformations including Formulas," IOGP Publication 373-7-2, Geomatics Guidance Note number 7, part 2, p. 142, 2004.

[44] T. Vincenty, "Direct and inverse solutions of geodesics on the ellipsoid with application of nested equations," Survey Review, XXII, Issue 176, pp. 88-93, doi:10.1179/sre.1975.23.176.88, 1975.

[45] T. Fukuda, Y. Ishihara, H. Ochi, M. Deguchi, N. Takahashi, K. Imai, M. Kido, Y. Ohta, M. Imano, S. Miyoshi, and H. Yamada, "Development of an on-demand monitoring buoy system for crustal deformation," BlueEarth Sympo., BE17-P69, CST Nihon University, Tokyo, 2017.

[46] R. Azuma, F. Tomita, T. Iinuma, M. Kido, and R. Hino, "Development and examination of new algorithm of traveltime detection in GPS/acoustic geodetic data for precise and automated analysis," Earth Planet Space, Vol.68, No.143, doi:10.1186/s40623-016-0521-2, 2016.

[47] C. Honsho and M. Kido, "Comprehensive analysis of traveltime data collected through GPS-acoustic observation of seafloor crustal movements," J. Geophys. Res., Vol.122, pp. 8583-8599, doi:10.1002/2017JB014733, 2017.

[48] M. Imano, M. Kido, Y. Ohta, N. Takahashi, T. Fukuda, H. Ochi, C. Honsho, and R. Hino, "Accuracy of real-time GPS/Acoustic measurement using a slackly moored buoy," JpGU-AGU joint meeting, SOG72-15, 2017.

[49] H. Ochi, Y. Ishihara, T. Fukuda, M. Deguchi, N. Takahashi, K. Imai, M. Kido, Y. Ohta, M. Imano, S. Miyoshi, and H. Yamada, "Development of an on-demand monitoring buoy system –acoustic data transfer for seafloor pressure gauge–," BlueEarth Symp., BE17-P70, 2017.

[50] H. Ochi, Y. Ishihara, and T. Sugiyama, "Concept of a tsunami warning buoy system and an acoustic telemetry system for high current area," 2012 Oceans-Yeosu, pp. 1-3, doi:10.1109/OCEANS-Yeosu.2012.6263646, 2012.

Name:
Motoyuki Kido

Affiliation:
Professor, International Research Institute of Disaster Science, Tohoku University

Address:
468-1 Aza-aoba, Aramaki, Aoba-ku, Sendai 980-8572, Japan

Brief Career:
1996- Research Fellow of Japan Society for the Promotion of Science, Ocean Research Institute, The University of Tokyo
2000- Research Fellow of Science and Technology Agency, Japan Agency for Marine-Earth Science and Technology
2003- Project Researcher, Kobe University Research Center for Inland Seas, Kobe University
2004- Project Researcher, Graduate School of Science, Tohoku University
2010- Associate Professor, Graduate School of Science, Tohoku University
2015- Professor, International Research Institute of Disaster Science, Tohoku University

Selected Publications:
• M. Kido et al., "Progress in the Project for Development of GPS/Acoustic Technique Over the Last 4 Years," GENAH, IAG Symposia, doi:10.1007/1345_2015_127, 2015.
• M. Kido et al., "Trench-normal variation in observed seafloor displacements associated with the 2011 Tohoku-oki earthquake," Geophys. Res. Lett., doi:10.1029/2011GL048355, 2011.

Academic Societies & Scientific Organizations:
• Seismological Society of Japan (SSJ)
• Geodetic Society of Japan (GSJ)
• American Geophysical Union (AGU)

Name:
Misae Imano

Affiliation:
Graduate Student, Graduate School of Science, Tohoku University

Address:
6-6 Aoba, Aramaki, Aoba-ku, Sendai 980-8578, Japan

Brief Career:
2016 Master of Science, Tohoku University
2016- Graduate Student, Graduate School of Science, Tohoku University

Selected Publications:
• M. Imano et al., "Improvement in the Accuracy of Real-time GPS/Acoustic Measurements Using a Multi-purpose Moored Buoy System by Removal of Acoustic Multipath," GENAH, IAG Symposia, doi:10.1007/1345_2015_192, 2015.

Academic Societies & Scientific Organizations:
• Seismological Society of Japan (SSJ)
• Geodetic Society of Japan (GSJ)
• American Geophysical Union (AGU)

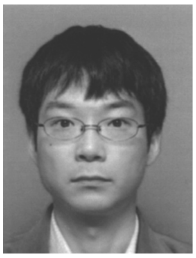

Name:
Yusaku Ohta

Affiliation:
Associate Professor, Research Center for Prediction of Earthquakes and Volcanic Eruptions, Graduate School of Science, Tohoku University

Address:
6-6 Aramaki-Aza-Aoba, Aoba-ku, Sendai 980-8578, Japan

Brief Career:
2007 Doctor of Science, Nagoya University
2007- Assistant Professor, Graduate School of Science, Tohoku University
2014- Associate Professor, Graduate School of Science, Tohoku University

Selected Publications:
• Y. Ohta et al., "Quasi real-time fault model estimation for near-field tsunami forecasting based on RTK-GPS analysis: Application to the 2011 Tohoku-Oki Earthquake (Mw9.0)," J. Geophys. Res., Vol.117, B02311, doi:10.1029/2011JB008750, 2012.
• Y. Ohta et al., "Geodetic constraints on afterslip characteristics following the March 9, 2011, Sanriku-oki earthquake, Japan," Geophys. Res. Lett., Vol.39, L16304, doi:10.1029/2012GL052430, 2012.
• Y. Ohta et al., "Large surface wave of the 2004 Sumatra-Andaman earthquake captured by the very long baseline kinematic analysis of 1-Hz GPS data," Earth Planets Space, Vol.58, No.2, pp. 153-157, 2006.

Academic Societies & Scientific Organizations:
• Seismological Society of Japan (SSJ)
• Geodetic Society of Japan (GSJ)
• American Geophysical Union (AGU)

Name:
Tatsuya Fukuda

Affiliation:
Engineer, Marine Technology and Engineering Center, Japan Agency for Marine-Earth Science and Technology

Address:
2-15 Natsushima-cho, Yokosuka 237-0061, Japan

Brief Career:
2009- Engineer, Japan Agency for Marine-Earth Science and Technology

Name:
Narumi Takahashi

Affiliation:
Principal Chief Researcher, National Research Institute for Earth Science and Disaster Resilience

Address:
3-1 Tennodai, Tsukuba 305-0006, Japan

Brief Career:
1995- Post-Doctoral Researcher, Ocean Research Institute, The University of Tokyo
1996- Joined Japan Marine Science and Technology Center (Japan Agency for Marine-Earth Science and Technology)
2014- Deputy Director, Japan Agency for Marine-Earth Science and Technology
2016- Deputy Director-General, Network Center for Earthquake, Tsunami and Volcano, National Research Institute for Earth Science and Disaster Resilience

Selected Publications:
- N. Takahashi et al., "Buoy platform development for observation of tsunami and crustal deformation," IAG Symposia Series, Springer, doi:10.1007/1345_2015_114, 2015.
- N. Takahashi et al., "Crustal structure of the Izu-Ogasawara island arc," J. Geography, Vol.124, No.5, p. 813, doi:10.5026/jgeography.124.813, 2015.

Academic Societies & Scientific Organizations:
- Seismological Society of Japan (SSJ)
- American Geophysical Union (AGU)

Name:
Satoshi Tsubone

Affiliation:
Engineer, Interlink Inc.

Address:
2-2-24 Mishiki, Naka-ku, Nagoya 460-0003, Japan

Brief Career:
1999- Interlink Inc.
2015- Japan Agency for Marine-Earth Science and Technology
2017- Interlink Inc.

Name:
Yasuhisa Ishihara

Affiliation:
Engineer, Ocean Observation Technology Group, Department of Marine technology Development, Marine Technology and Engineering Center, Japan Agency for Marine-Earth Science and Technology

Address:
2-15 Natsushima-cho, Yokosuka 237-0061, Japan

Brief Career:
1992- Mitsubishi Heavy Industries, Ltd.
2001- Assigned Employee, Japan Marine Technology Center (Japan Agency for Marine-Earth Science and Technology)
2006- Joined Japan Agency for Marine-Earth Science and Technology
2012- Group Leader, Marine Technology and Engineering Center, Japan Agency for Marine-Earth Science and Technology

Selected Publications:
- Y. Ishihara, and K. Mizuno, "JAMSTEC'S m-TRITON: Surface High-Speed Data Transmission," ARGOS Forum, 69, p. 10, 2010.

Academic Societies & Scientific Organizations:
- Japan Society of Applied Physics (JSAP)

Name:
Hiroshi Ochi

Affiliation:
Coordinator, Marine Technology and Engineering Center, Japan Agency for Marine-Earth Science and Technology

Address:
2-15 Natsushima-cho, Yokosuka 237-0061, Japan

Brief Career:
1990- Joined Japan Agency for Marine-Earth Science and Technology (JAMSTEC)
2001- Guest Staff, University of Newcastle upon Tyne
2009- Group Leader, Marine Technology and Engineering Center, Japan Agency for Marine-Earth Science and Technology
2017- Coordinator, Marine Technology and Engineering Center, Japan Agency for Marine-Earth Science and Technology

Selected Publications:
• H. Ochi, Y. Watanabe, and T. Shimura, "A Measurement of Absorption Loss at 80 kHz Band for Wideband Underwater Acoustic Communication," Jpn. J. Appl. Phys., doi:10.1143/JJAP.47.4366, 2008.

Academic Societies & Scientific Organizations:
• Institute of Electrical and Electronics Engineers (IEEE)
• Marine Acoustics Society of Japan (MASJ)
• Acoustical Society of America (ASA)

Name:
Kentaro Imai

Affiliation:
Research Scientist, Research and Development Center for Earthquake and Tsunami, Japan Agency for Marine-Earth Science and Technology

Address:
3173-25 Showa-machi, Kanazawa-ku, Yokohama 236-0001, Japan

Brief Career:
2008- Project Researcher, The Center for Integrated Disaster Information Research, Earthquake Research Institute, The University of Tokyo
2010- Assistant Professor, Disaster Control Reserch Center, Tohoku University
2012- Assistant Professor, International Research Institute of Disaster Science, Tohoku University
2015- Research Scientist, Japan Agency for Marine-Earth Science and Technology

Selected Publications:
• T. Baba, S. Allgeyer, J. Hossen, P. R. Cummins, H. Tsushima, K. Imai, K. Yamashita, and T. Kato, "Accurate numerical simulation of the far-field tsunami caused by the 2011 Tohoku earthquake," including the effects of Boussinesq dispersion, seawater density stratification, elastic loading, and gravitational potential change, OCEAN MODELLING, Vol.111, pp. 46-54, doi:http://dx.doi.org/10.1016/j.ocemod.2017.01.002, 2017.

Academic Societies & Scientific Organizations:
• Japan Society of Civil Engineers (JSCE)
• Japan Society for Natural Disaster Science (JSND)

Name:
Chie Honsho

Affiliation:
Project Researcher, Research Center for Prediction of Earthquakes and Volcanic Eruptions, Graduate School of Science, Tohoku University

Address:
6-6 Aza-Aoba, Aramaki, Aoba-ku, Sendai 980-8578, Japan

Brief Career:
1999 Doctor of Science, The University of Tokyo
2006- Post-Doctoral Researcher, School of Engineering, The University of Tokyo
2011- Post-Doctoral Researcher, Atmosphere and Ocean Research Institute, The University of Tokyo
2015- Program-Specific Assistant Professor, International Research Institute of Disaster Science, Tohoku University
2017- Project Researcher, Research Center for Prediction of Earthquakes and Volcanic Eruptions, Tohoku University

Selected Publications:
• C. Honsho and M. Kido, "Comprehensive analysis of traveltime data collected through GPS-acoustic observation of seafloor crustal movements," J. Geophys. Res., Vol.122, pp. 8583-8599, doi:10.1002/2017JB014733, 2017.
• C. Honsho et al., "High-resolution acoustic mapping to understand the ore deposit in the Bayonnaise knoll caldera, Izu-Ogasawara arc," J. Geophys. Res. Solid Earth, Vol.120, doi:10.1002/2014JB011569, 2015.

Academic Societies & Scientific Organizations:
• Geodetic Society of Japan (GSJ)

Name:
Ryota Hino

Affiliation:
Professor, Research Center for Prediction of Earthquakes and Volcanic Eruptions, Graduate School of Science, Tohoku University

Address:
6-6 Aza-Aoba, Aramaki, Aoba-ku, Sendai 980-8578, Japan

Brief Career:
1992 Doctor of Science, Tohoku University
1992- Research Associate in Faculty of Science, Tohoku University
1998- Associate Professor in Graduate School of Science, Tohoku University
2013- Professor in International Research Institute of Disaster Science, Tohoku University
2015- Professor in Graduate School of Science, Tohoku University

Selected Publications:
• R. Hino et al., "Was the 2011 Tohoku-Oki earthquake preceded by aseismic preslip? Examination of seafloor vertical deformation data near the epicenter," Mar. Geophys. Res., Vol.35, pp. 181-190, doi:10.1007/s11001-013-9208-2, 2014.
• R. Hino et al., "Hypocenter distribution of main- and aftershocks of the 2005 Off Miyagi Prefecture Earthquake located by ocean bottom seismographic data," Earth Planets Space, Vol.58, pp. 1543-1548, 2006.

Academic Societies & Scientific Organizations:
• Seismological Society of Japan (SSJ)
• Geodetic Society of Japan (GSJ)
• American Geophysical Union (AGU)